Effect of the crystal structure on the optical properties and Ag sensitization of Tb^{3+}/Yb^{3+} ions in silica-zirconia glasses and glass-ceramics

F. Enrichi*[a,b], M. Cassetta[a], N. Daldosso[a], E. Cattaruzza[c], P. Riello[c], R. Zairov[d], A. Vomiero[c,e], G. C. Righini[f],

[a] Department of Computer Science, University of Verona, Ca' Vignal 2, Strada Le Grazie 15, 37134 Verona, Italy
[b] ISP-CNR Institute of Polar Sciences, Via Torino 155, 30172 Mestre, Venezia, Italy
[c] Department of Molecular Sciences and Nanosystems, Ca' Foscari University of Venezia, Via Torino 155, 30172 Mestre, Venezia, Italy
[d] Arbuzov Institute of Organic and Physical Chemistry, FRC Kazan Scientific Center, Russian Academy of Sciences, Arbuzov str., 8, 420088, Kazan, Russian Federation
[e] Division of Materials Science, Department of Engineering Sciences and Mathematics, Luleå University of Technology, 971 87 Luleå, Sweden
[f] CNR-IFAC Nello Carrara Institute of Applied Physics, Via Madonna del Piano 10, 50019 Sesto Fiorentino, Firenze, Italy

* corresponding author e-mail: francesco.enrichi@univr.it

Abstract

The role of the material structure in the energy transfer between Ag and Tb^{3+}/Yb^{3+} ions is studied in silica-soda-zirconia sol-gel glasses and glass-ceramics. The preparation of Tb^{3+} and Yb^{3+} doped silica-soda-zirconia layers was carried out by sol-gel and dip-coating, followed by thermal annealing. The precipitation of zirconia nanocrystals was obtained by controlling the annealing temperature: from a full amorphous glass at 700°C into a glass-ceramic at 1000°C. A different crystalline structure of zirconia nanocrystals, tetragonal or cubic, was controlled by the rare-earth doping and investigated in relation to the Tb^{3+}/Yb^{3+} optical properties. Moreover, Ag codoping was introduced by ion-exchange, obtaining a significant photoluminescence enhancement, both in the intensity and in the broadness of the excitation band, covering the whole UV region and part of the violet-blue region. Ag-sensitized Tb^{3+}/Yb^{3+} doped silica-soda-zirconia glass-ceramics were attested to be potential candidates for energy-related applications, such as spectral conversion layers for solar cells, lasers and light-emitting devices (LEDs) in the visible and NIR spectral regions.

Keywords: Sol-gel, glass-ceramics, Tb^{3+}/Yb^{3+} ions, Ag sensitizers, cubic zirconia, tetragonal zirconia, nanocrystals, NIR emitters.

1. Introduction

Rare earth ions RE^{3+} have been widely used as active species in optical materials for photon emission and spectral manipulation thanks to their peculiar spectral properties, due to the number and distribution of the available energy levels and long excited state lifetimes [1]. A detailed review on the optical applications of rare earth oxides has been recently reported by Hossain et al. [2], spanning from photovoltaics to lighting and photonics. However, a major concern in the optical efficiency of RE^{3+} doped materials is the occurrence of non-radiative transitions that lead to undesirable energy dissipation. Among the quenching mechanisms, multi phonon relaxation plays a

major role. It consists in the simultaneous creation of several phonons, which can equal the energy of the transition between the excited level and the next lower level. Since the probability for multiphonon decay decreases exponentially with the number of required phonons, it is desirable to surround the active ion by a matrix that possesses low vibrational energies [3]. In glasses, the highest energy vibrations are stretchings of the anions against the glass forming cations, whose frequency varies with the glass composition, spanning from bromide and chalcogenides (200 – 300 cm^{-1}) to silica (1000 – 1100 cm^{-1}). Moreover, the presence of residual -OH species increases the non-radiative decay rates, because of coupling between the RE states and the high energy stretching vibrations of the OH groups (~3200 cm^{-1}). Crystalline materials can offer better properties than glasses in terms of transparency, optical cross-sections and non-radiative relaxation rates, but they don't have the same chemical and mechanical stabilities and fabrication ease. Between these two extremes, glass-ceramics is constituted by a crystalline phase dispersed within a glass matrix [4,5]. Glass ceramics can be obtained by a controlled nucleation and crystallization of nanometric-sized grains by separation from the amorphous phase. EXAFS studies indicate that RE^{3+} ions in these materials tend to be incorporated into the ceramic nanocrystals [4–8], providing better spectroscopic properties, higher solubilities and lower phonon energies which lead to reduced non-radiative recombination rates with respect to their glassy counterpart. A direct comparison between the glass and the corresponding glass-ceramic with the same chemical composition was reported for Tb^{3+}/Yb^{3+} rare earth ions in silica-hafnia (70% SiO_2 – 30% HfO_2) [9–11], demonstrating a significant increase in the maximum energy transfer efficiency from Tb^{3+} ions to Yb^{3+} ions, being about 60% in the glass and 90% in the glass-ceramic [11]. Tb^{3+} and Yb^{3+} have often been combined for downconversion, with the aim of increasing the efficiency of silicon solar cells. In fact, Yb^{3+} emission in the range 950-1150 nm is close to the silicon bandgap, which corresponds to 1120 nm for c-Si (Eg = 1.11 eV at 300 K). However, due to its simple energy-level structure, with only two manifolds in the 4*f* orbital, the $^2F_{7/2}$ ground state and $^2F_{5/2}$ excited state [12,13], Yb^{3+} has no absorption in the UV-visible range, therefore co-doping with other lanthanides [9–11,14–19] was demonstrated to provide alternative excitation paths by energy-transfer, with the additional possibility of photon multiplication by quantum cutting. Silver was also reported as an efficient broadband sensitizer for several RE^{3+} ions (Sm, Eu, Tb, Dy, Er, Yb) [20–31], and recently our group explored the possibility to combine the effect of silver broadband enhancement with the quantum-cutting potential of Tb^{3+}/Yb^{3+} coupling in silica-zirconia glass-ceramics [32–34]. Zirconia has a lower maximum phonon energy than silica [35] and higher refractive index. In this context, the control of the crystalline phase offers an additional element to tune these properties by changing the bandgap, the density of states and the phonon energies [36]. Therefore, in this paper we further investigate the role of the glass-ceramic matrix and its crystalline structure on the optical properties of the composite material, towards the realization of more efficient optical devices.

2. Materials and methods

Undoped, Tb doped (1 mol.%) and Tb/Yb co-doped (1 mol% Tb / 4 mol.% Yb) films of nominal molar composition 70% SiO_2 – 30% ZrO_2 and additional 2,5% Na_2O were prepared by sol–gel technique and deposited by dip-coating. Tetraethyl orthosilicate $Si(OC_2H_5)_4$ (TEOS) and zirconium propoxide $Zr(OC_3H_7)_4$ (ZPO) were used as precursor for silica and zirconia respectively. TEOS was dissolved in ethanol (EtOH) and hydrolized with H_2O and HCl (TEOS : HCl : H2O : EtOH = 1 : 0.01

: 2 : 25, Sol.Si). For Tb (1 mol%) and Yb (4 mol%) doped samples, terbium and ytterbium nitrates $Tb(NO_3)_3$ and $Yb(NO_3)_3$ were added to the solution (Sol.Si-RE) and then left stirring for 1 h. In the meanwhile, ZPO was mixed with acetylacetone (Acac) and ethanol (ZPO : Acac : EtOH = 1 : 0.5 : 50, Sol.Zr) and sodium acetate was dissolved in methanol (60 mg/ml, Sol.Na). The deposition solution has been obtained by mixing Sol.Si-RE with Sol.Zr and adding dropwise Sol.Na at room temperature. The solution has been left stirring at room temperature overnight for 16 h.

Multi-layer films have been deposited on fused silica substrates by dipping. Each layer was annealed in air at 700 °C for 3 min. A final heat treatment in air at 700 °C (glass, G) or 1000 °C (glass-ceramic, GC) for 1 h was performed after the deposition of the last single layer. The typical thickness of each single layer after heat treatment was about 40 nm. By this process we realized 10 layers crack-free films with a total thickness of about 400 nm. To introduce silver in the films, Ag+↔Na+ ion-exchange was performed by immersing the samples in a molten salt bath (1 mol.% AgNO3 in NaNO3) at 350 °C for 1 h. After ion exchange, the samples were annealed for 1 h at 380 °C or 430 °C in air, to induce migration and aggregation of the metal ions. The sample name is coded as GX-L for glasses and GCX-L for glass-ceramics, with X=1 (1% Tb), X=4 (4% Yb), X=5 (1% Tb + 4% Yb) and L=A (Ag exchanged), L=B (Ag exchanged and annealed at 380 °C), L=C (Ag exchanged and annealed at 430 °C). When L is not indicated the sample is not exchanged.

Compositional and structural information of the samples by Rutherford Backscattering Spectrometry (RBS) and Transmission Electron Microscopy (TEM) was already reported on a previous paper [34]. Additional structural and optical characterization of the films were obtained by X-Ray Diffraction (XRD), Raman Spectroscopy and Photoluminescence Spectroscopy.

RBS was carried out using a 2.2 MeV $4He^+$ beam at 160° backscattering angle in IBM geometry. RUMP code was used for the analysis of the experimental spectra [37]. The conversion from areal density (the natural unit of measurement for RBS) to film thickness is based on a molar density of the film equal to a weighted average between silica (2.00 g cm^{-3}) and zirconia (5.68 g cm^{-3}), according to the nominal stoichiometric composition of the matrix (70 SiO_2 – 30 ZrO_2), confirmed by the RBS analysis.

XRD measurements for crystal phase identification were done at room temperature by an X'Pert PRO diffractometer (Panalytical). A Cu anode equipped with Ni filter was used as radiation source (Kα radiation, λ=1.54056 Å). Diffractograms were collected both in Bragg-Brentano geometry and in grazing incidence, using a step-by-step scan mode in the 2θ range 10°–100°, with a scanning step of 0.05° and counting time of 30 s/step. Nanocrystal size was determined by Line Broadening Analysis (LBA), in particular by using the Warren-Averbach method [38].

Raman measurements were carried out in back-scattering geometry at room temperature on polished samples using a triple-axis monochromator (Horiba Jobin-Yvon, model T-64000) set in a double subtractive single configuration. The scattered radiation was filtered by three holographic gratings (1800 lines/mm) and detected with a CCD detector (1024x256 pixels) cooled by liquid nitrogen. The exciting radiation was provided by a mixed Ar-Kr ion gas laser (Spectra Physics Satellite 2018 RM) set at 514.5 nm, thus allowing a resolution of about 0.6 cm^{-1}/pixel. The laser beam was focused onto a spot of 1 μm by using a 100x objective with N.A. = 0.95. The power on the sample surface was fixed at about 10 mW. Samples were optically inspected before and after the measurements without observing appreciable alteration on the μm-length scale. Measurements of the Stokes-shifted spectra, in the wavenumber region between 10 and 1250 cm^{-1}, were acquired in parallel (HH) and crossed

(HV) polarization. Each spectrum was corrected by subtracting air-scattering, occurring in the low-wavenumber region below 180 cm^{-1}, and a linear baseline, extending over the full spectral range, to account for the weak luminescence background.

Photoluminescence excitation (PLE) and emission (PL) spectra were recorded by a FLS980 Photoluminescence Spectrometer (Edinburgh Instruments). A continuous-wave xenon lamp was used as excitation sources for steady-state measurements, coupled to a double-grating monochromator for wavelength selection. The light emitted from the sample was collected through a double-grating monochromator was recorded by a photon counting R5509-73 PMT cooled at -80 °C (NIR range).

3. Results and discussion

The elemental composition of the G and GC series before and after Ag introduction and annealing was studied by RBS, as discussed in a previous publication [34]. The analysis confirmed for all the samples the nominal silica, zirconia and soda composition, as well as the doping with Tb, Yb and Ag. Moreover, Tb/Yb doped films exhibited flat in-depth concentration profiles for the dopants, indicating compositional homogeneity and uniformity of the sol-gel deposition process. $Ag^{+}\leftrightarrow Na^{+}$ ion-exchanged samples showed about 5% Ag introduction in glasses (G) and 2% in glass-ceramics (GC). The higher amount of silver in the G matrix with respect to GC was also discussed in [34], and attributed to the lower density, higher disorder, larger presence of non-bridging oxygens and defectivity of the glass with respect to the multicrystalline glass-ceramic.

Additionally, HR-TEM analysis confirmed the precipitation of zirconia crystalline nanoparticles in glass-ceramics and eventually a few Ag metal nanoparticles were found in Ag-exchanged 430 °C annealed glasses, due to the higher concentration and higher mobility of silver in the amorphous material.

To deeper analyse the crystalline structure of the films, XRD, Raman and photoluminescence spectroscopy are discussed and compared in this manuscript. **Figure 1** (a) and (b) reports the XRD reflections of the synthesized G and GC samples respectively, confirming the transition from an amorphous phase (G) to a glass-ceramic composite (GC) for 1000 °C annealed samples. Tetragonal-phase ZrO_2 (*t*-ZrO_2) nanocrystals were detected in the undoped and Tb-doped GC samples (GC0 and GC1), while cubic-phase ZrO_2 (*c*-ZrO_2) nanocrystals were observed for Yb-doped and Tb/Yb co-doped samples (GC4 and GC5), attested by the different shape of the observed reflection peaks, especially those at $2\theta \approx 35.5°$ (200) and $2\theta \approx 75°$ (400), expanded in **Figure 1** (c). These reflections exhibit single peaks in the cubic phase, which split in two components in the tetragonal phase. Unusual relative intensities of the observed diffraction peaks supported by comparing the reflections in Theta-2Theta geometry with the ones in grazing incidence geometry in **Figure 1** (d) may be due to a preferential orientated growth of the zirconia nanocrystals along the [110] direction. For GC samples, the zirconia nanocrystal size was determined by Line Broadening Analysis (LBA) [38]. The calculated mean crystallite size was about 14 nm for tetragonal zirconia and about 12 nm for cubic zirconia, with a broad distribution from 5 nm to 25 nm [34]. As an example, the crystal size distribution calculated on GC5 sample is reported in **Figure 1** (e).

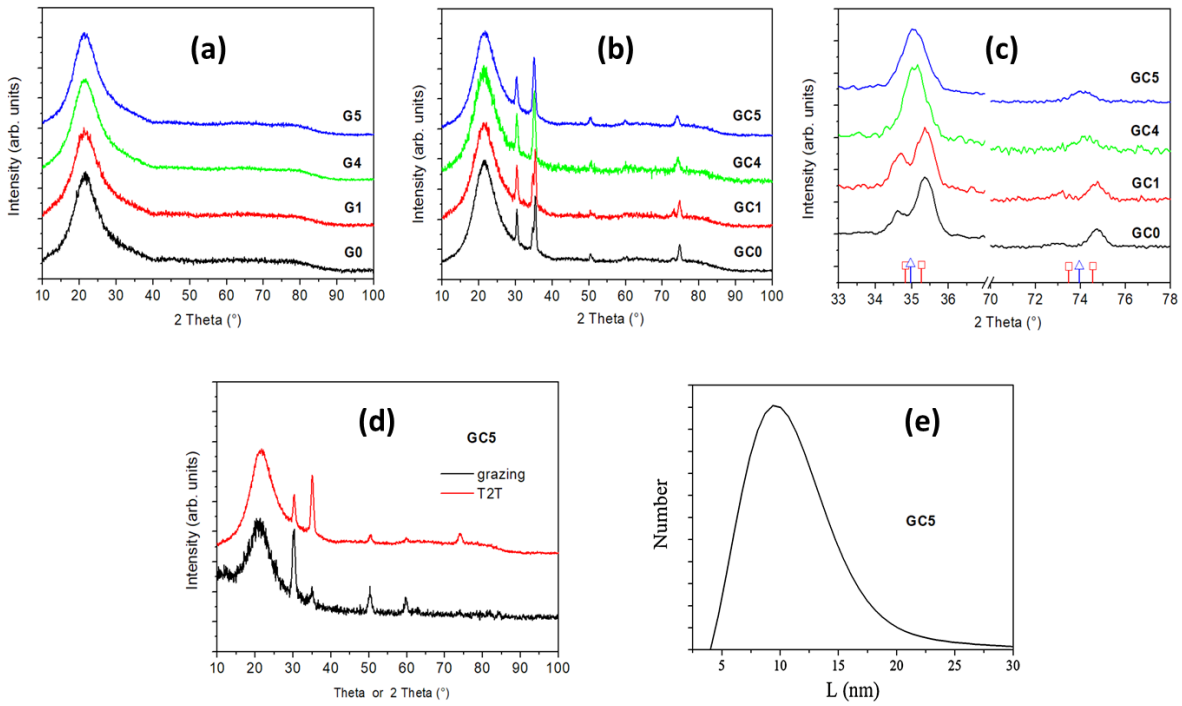

Figure 1. XRD analysis on silica-zirconia-soda samples: (a) G samples; (b) GC samples; (c) single or double peak XRD reflections reveal a cubic (GC4 and GC5 samples) or tetragonal (G0 and G1) crystal phase; (d) intensity comparison in Theta-2Theta geometry or in grazing incidence; (e) example of crystal size distribution calculated on GC5 sample by Line Broadening Analysis (LBA) [38]. Modified reproduction from [34].

A deeper analysis of the crystalline parameters is related to the position of the diffraction peaks, as compared to the nominal positions of tetragonal and cubic zirconia. In **Table 1** the nominal peak positions and the experimental positions are compared.

Table 1. Peak positions and shifts from the nominal values for the glass-ceramic samples

Tetragonal ZrO_2	GC0 sample		GC1 sample	
Nominal peak position	Measured peak position	Difference	Measured peak position	Difference
34,8132	34.60 ± 0.05	– 0.21 ± 0.05	34.60 ± 0.05	– 0.21 ± 0.05
35,2539	35.35 ± 0.05	+ 0.10 ± 0.05	35.35 ± 0.05	+ 0.10 ± 0.05
73,4632	73.10 ± 0.05	– 0.36 ± 0.05	73.10 ± 0.05	– 0.36 ± 0.05
74,5358	74.75 ± 0.05	+ 0.21 ± 0.05	74.75 ± 0.05	+ 0.21 ± 0.05

Cubic ZrO_2	GC4 sample		GC5 sample	
Nominal peak position	Measured peak position	Difference	Measured peak position	Difference
34,9601	35.05 ± 0.05	+ 0.09 ± 0.05	35.05 ± 0.05	+ 0.09 ± 0.05
73,9412	74.10 ± 0.05	+ 0.16 ± 0.05	74.10 ± 0.05	+ 0.16 ± 0.05

IT WOULD BE GOOD TO DISCUSS XRD PEAKS SHIFT…. IS IT POSSIBLE TO CALCULATE THE CELL SIZE AND DEFORMATION AND EXPLAIN THE COMPRESSION OR EXPANSION OF THE DIFFERENT PLANES?

The structural properties of zirconia nanocrystals have been widely studied in literature. Bulk zirconia adopts a monoclinic crystal structure at room temperature, and it transforms to tetragonal (1170 °C) and cubic (2370 °C) at higher temperatures. However, the high surface energy of nanocrystalline size particles and/or the addition of dopants to the structure are crucial aspects for the stabilization of the tetragonal and cubic phase even at room temperature. Examples are the well-known yttria stabilized zirconia (YSZ) and the use of other trivalent or quadrivalent dopants like Ca, Ce, Fe, Ga, Gd, Ge, Nb, Sc [39–42]. Furthermore, novel orthorhombic phase stabilization was recently reported by Ta doping [43]. The closest example to our system was reported a few years ago for the specific case of Tb^{3+} doped zirconia nanophosphors, showing that increasing the molar concentration above 5% induces a cubic phase stabilization, while below that amount a tetragonal phase is observed [44]. Therefore, the phase stabilization in GC samples can be attributed to a combination of different factors, including the size of the zirconia nanocrystals, the nature of the dopant ions and the amount of doping, keeping into account that this amount may be significantly increased from the nominal average doping by the fact that RE^{3+} ions are incorporated in the nanocrystals during the annealing process [4,7,8].

XRD analysis of Ag exchanged samples are reported in **Figure 2** for G (a) and GC (b). It is worth noticing the presence of a narrow peak at about 32.2 °, which is associated to AgO crystals. In the G matrix the higher mobility of silver allows an easier penetration in the whole sol-gel layer, resulting in a higher final concentration, as attested by the compositional analysis. After annealing the narrowing of the diffraction peak and the increasing of the intensity suggests an improvement of the AgO structure. In these samples RBS characterization reported migration and accumulation of silver towards the surface, which contributes to the consolidation of this peak. On the contrary, in GC samples the AgO peak disappears after annealing. RBS characterization did not evidence any effect of silver migration and accumulation in the concentration profile, which essentially remains unchanged after annealing, therefore the disappearing of the peak seems associated to a local rearrangement influenced by the presence of zirconia.

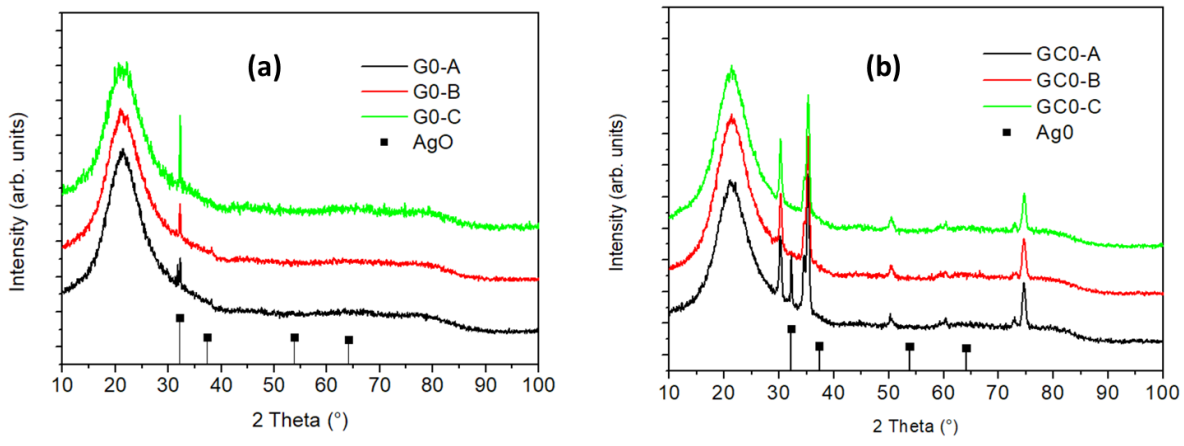

Figure 2. XRD analysis on silica-zirconia-soda undoped samples after Ag exchange and annealing: (a) G samples; (b) GC samples.

The HV Raman spectra of glasses, reported in **Figure 3**, show their amorphous profile starting from the typical excess of states in the low frequency region (10-150 cm^{-1}), namely the boson peak (BP) with its maximum located at about 50 cm^{-1}. The band at about 800 cm^{-1}, arising from the three-fold degenerate "rigid cage" vibrational mode of SiO_4 units [45], does not show any appreciable spectral change among the glasses and glass-ceramic samples (see **Figure 3** (a) and (b)).

The other typical bands of silicate glasses (R, D_1, D_2 and their tail in the range 200-550 cm^{-1}) were not considered on our analysis since their strong intensity would hide the different polymorphs of crystalline zirconia Raman peaks (in particular for the case of *c*-ZrO_2) [46,47]. However, being strongly polarized in the HV spectra these contributions turn out inactive, providing the best option in evaluating our glass-ceramics with low crystallinity [48].

Remarkable differences among different glasses rise in the high frequency region where the vibrations are mostly due to the intrinsic vibrational modes of the tetrahedral units (TO_4). The centroid area and width of these bands reflect the polymerization degree of the glass, which is ruled by the abundance and species of the network modifier (NM) cations as well as the charge balancing ones. The G0 glass shows a spectrum quite similar to that of silica (inset of **Figure 3** (a)) with exception of the high frequency band peaked at about 960 cm^{-1}, probably due to the effect of ZrO_2 involved in the Si-O-Zr linkage. This band was already observed and assigned to glasses with similar composition experiencing the same thermal treatment (700 °C), thus ruling out any effect of the Si-O-H linkages due to variable concentrations of structural H_2O which is typical of sol-gel-derived glasses [49]. The doped glasses G1, G4 and G5 show altogether a higher intensity in the high frequency region mirroring perhaps strong variations in the T-O-T angle the incursion of RE within the glass network. This effect is similar to that of a soda-lime silicate glass doped with different RE investigated in [50]. However, for such a case the effect played by the RE doping is to depolymerize the glass network thereby increasing the non-bridging oxygen species within the structure. As a matter of fact, the decreasing of viscosity of their parental melts confirms this assumption [51].

The *t*-ZrO_2 modes of the GC0 and GC1 HV spectra, were identified in their typical positions at about 270 cm^{-1} (A_{1g}); 314 and 600 cm^{-1} (B_{1g}); 455, 645 cm^{-1} and the weakest one at 147 cm^{-1} being probably hidden by the boson peak tail and they are assigned to the E_g modes. The assignations of the above modes are reported in ref. [52].

Samples GC4 and GC5 display the typical mode (F_{2g}) of the *c*-ZrO_2 as similarly reported in refs. [35,48,53], peaked at about 620 cm^{-1} in our samples.

Figure 3 (c) shows typical cross-polarized (HV) LOFIRS (Low Frequency Inelastic Raman Scattering) spectra carried out from the glass surface. The HR spectra consist of a broad and asymmetric bump peaked at about 15.2 cm^{-1}. This peak is originated by the Raman active spheroidal vibrational modes of Ag nanoclusters embedded/incorporated into the glass matrix as theorized in the seminal work of Lamb [54,55]. The l=0 and l=2 particle modes are characterized by typical frequencies ($\boldsymbol{\omega}$) which are proportional to the inverse of the particle diameter. Starting from the material sound velocities (transverse v_t and longitudinal v_l) is possible to estimate the diameter via relation [54]:

$$\boldsymbol{\omega_0} = \frac{\mathbf{0.847}\boldsymbol{v_t}}{\boldsymbol{dc}}$$

Here d is the nanoparticle diameter, c is the light velocity in vacuum, whilst v_t = 1660 m/s is the transvers sound velocities in metallic silver. Through this equation we estimate a particle diameter of about 3.2 nm.

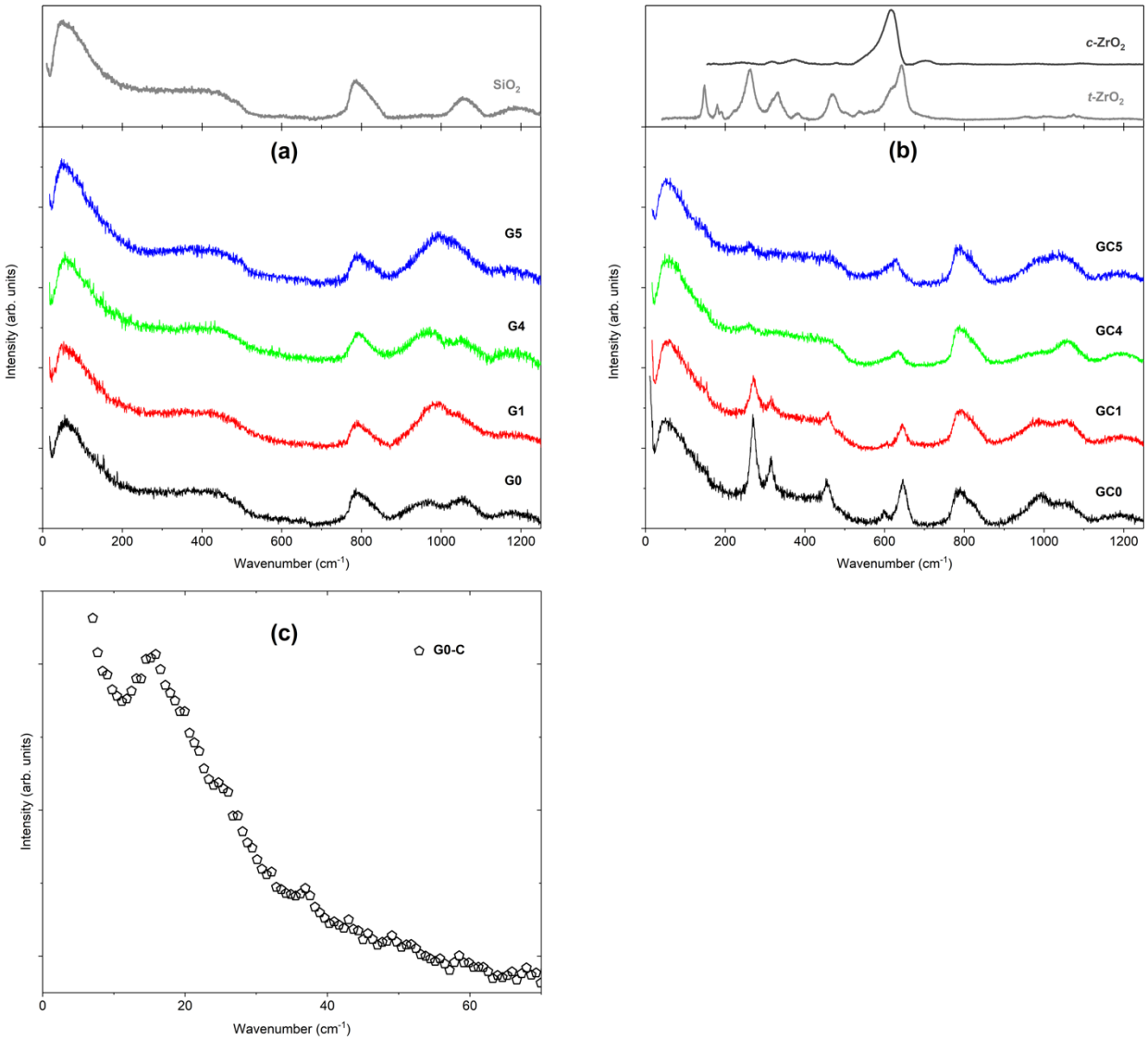

Figure 3. Raman HV Raman spectra of glasses (a) and glass-ceramics (b). The inset in (a) reports SiO_2 glass HV spectra for comparison, analogously as the inset in (b) which shows two reference spectra of the cubic (R040142) and tetragonal zirconia. (c) HV LOFIRS spectra probed in representative sample G0-C.

The optical properties of the prepared films were studied by means of PL spectroscopy to get insights into the materials structure and the optical efficiency. The normalized PL spectra of the glass and glass-ceramic samples after Ag-exchange and annealing reports the typical Tb^{3+} transitions from the $^5D_4$ excited state to the $^7F_6$ (488 nm), $^7F_5$ (542 nm), $^7F_4$ (582 nm) and $^7F_3$ (620 nm) ground state multiplets, as shown in **Figure 4** (a), with a zoom in the region of the main $^5D_4 \rightarrow {}^7F_5$ peak in **Figure 4** (b). It is worth noticing that the same spectral shape was observed for the samples without Ag

exchange. The spectral shapes highlight a different crystalline environment surrounding the terbium atoms, evolving from amorphous (G1-C, G5-C) to crystalline phase (GC1-C, GC5-C). Moreover, the different crystal peaks agree with a structural difference between *t*-ZrO_2 and *c*-ZrO_2. The additional side peak observed in Yb^{3+} co-doped sample attests the formation of new Tb^{3+} crystal sites, in agreement with the observations reported by other authors [56]. The structural modification is also supported by anomalous lifetime evolution, shown in **Figure 4** (d) for the crystalline material, where the addition of Yb^{3+} increases the mean lifetime in contrast with the expected Tb-Yb energy transfer that should decrease its value, as it occurs in the glassy material shown in **Figure 4** (c).

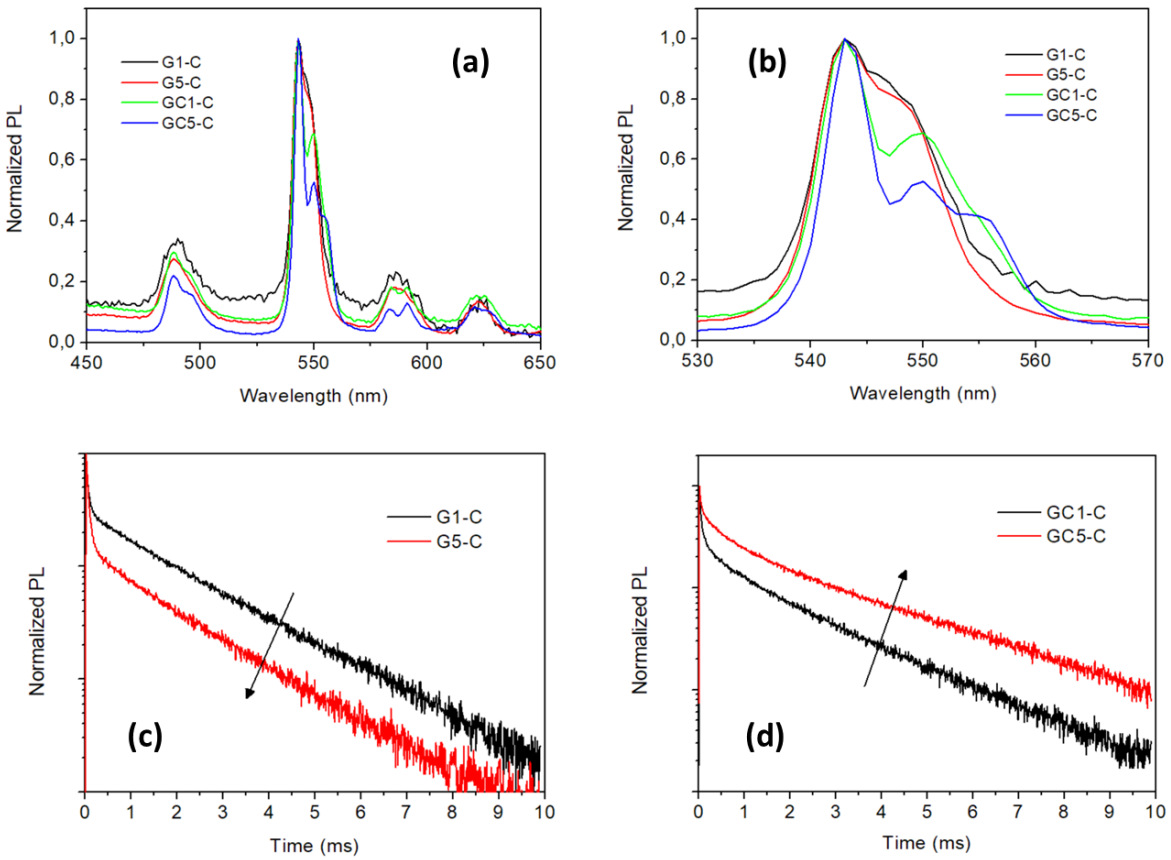

Figure 4. Normalized PL emission spectra (exc. 280 nm) of the glass and glass-ceramic samples after Ag-exchange and annealing (a), with a zoom on the main transition peak (b). Time resolved normalized PL intensity for the glass (c) and glass-ceramic (d) samples (exc. 280 nm, em. 543 nm).

The ceramic structure previously analysed and investigated is of paramount importance for the optical properties and Ag sensitization of the Tb^{3+}/Yb^{3+} codoped films. This is a fundamental aspect to keep into account when optimizing the materials properties towards possible applications, and it constitutes an additional value of glass-ceramics, with the possibility to further control and tune their desired properties. To this respect, we recently reported a detailed photoluminescence study on Ag sensitized Tb^{3+}/Yb^{3+} glasses and glass-ceramics [34]. **Figure 5**, reproduced under Creative Commons CC-BY license from that paper, demonstrates the superior performances of glass-ceramics with respect to glasses, and the possibility to obtain an efficient broadband downconversion from the UV-blue spectral region to the NIR, with high potential for silicon solar cells.

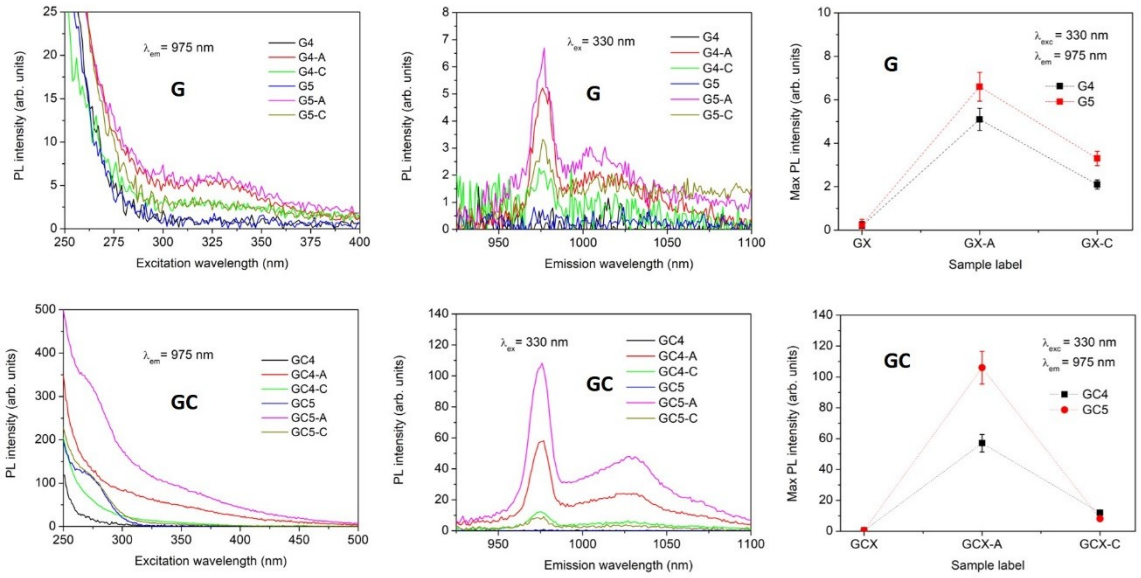

Figure 7. PL excitation (left column: λ_{em} = 975 nm), PL emission (centre column: λ_{exc} = 330 nm) and maximum PL intensity (right column: λ_{exc} = 330 nm, λ_{em} = 975 nm) of G (top row) and GC (bottom row) samples, indicating an efficient broadband enhanced excitation for Yb^{3+} ions after Ag exchange. Reproduced under Creative Commons CC-BY license from [34].

4. Conclusions

This paper is focused on understanding the impact of the crystal structure on the optical properties and Ag sensitization of Tb^{3+}/Yb^{3+} ions in silica-zirconia glasses and glass-ceramics. Sol-gel films with the same composition were annealed at 700 °C or 1000 °C. In the latter case, zirconia nanocrystals (about 12-14 nm in size) were formed by separation from the silica amorphous matrix. A significant structural role of RE^{3+} ions on the nanocrystal phase was observed, showing the stabilization of *c*-ZrO_2 for Yb^{3+} doped samples, instead of *t*-ZrO_2 for lower Tb^{3+} concentrations and for undoped samples. This was confirmed by XRD, Raman and PL spectroscopy.

Moreover, due to the higher mobility, Ag doping obtained by ion-exchange was higher in glasses than in glass-ceramics resulting for both the systems in a significant enhancement of RE^{3+} luminescence. In particular, in the NIR spectral range the crystalline glass-ceramic matrix significantly overcame the performance of the amorphous glass, in relation to the lower phonon energy and smaller number of non-radiative defects. Ag-enhanced Yb^{3+} PL showed a broadband excitation up to 400 nm for glass and 500 nm for glass-ceramics. These spectral regions are completely ineffective without Ag due to the lack of absorbing energy levels, with an absolute PL intensity about 16 times higher in glass-ceramics with respect to glass. Finally, the superior optical properties of *c*-ZrO2 were attested by PL lifetime analysis.

In conclusion, this work highlights the role of materials structure and Ag-enhancement to boost the optical emission of Tb^{3+}/Yb^{3+} glass-ceramic films, in particular in the NIR spectral range, with great potential for increasing the efficiency of silicon solar cells.

References

[1] A. Meijerink, R. Wegh, P. Vergeer, T. Vlugt, Photon management with lanthanides, Opt. Mater. (Amst). 28 (2006) 575–581. doi:10.1016/j.optmat.2005.09.055.

[2] M. Khalid Hossain, S. Hossain, M.H. Ahmed, I. Khan, N. Haque, G.A. Raihan, A Review on Optical Applications, Prospects, and Challenges of Rare-Earth Oxides, Cite This ACS Appl. Electron. Mater. 2021 (2021) 3715–3746. doi:10.1021/acsaelm.1c00682.

[3] T. Miyakawa, D.L. Dexter, Phonon sidebands, multiphonon relaxation of excited states, and phonon-assisted energy transfer between ions in solids, Phys. Rev. B. 1 (1970) 2961–2969. doi:10.1103/PHYSREVB.1.2961.

[4] M.C. Gonçalves, L.F. Santos, R.M. Almeida, Rare-earth-doped transparent glass ceramics, Comptes Rendus Chim. 5 (2002) 845–854. doi:10.1016/S1631-0748(02)01457-1.

[5] Y. Teng, K. Sharafudeen, S. Zhou, J. Qiu, Glass-ceramics for photonic devices, J. Ceram. Soc. Japan. 120 (2012) 458–466. doi:10.2109/jcersj2.120.458.

[6] N.D. Afify, G. Dalba, F. Rocca, XRD and EXAFS studies on the structure of Er3+-doped SiO2-HfO2 glass-ceramic waveguides: Er3+-activated HfO2 nanocrystals, J. Phys. D. Appl. Phys. 42 (2009) 115416. doi:10.1088/0022-3727/42/11/115416.

[7] F. Auzel, Rare Earth Doped Vitroceramics: New, Efficient, Blue and Green Emitting Materials for Infrared Up-Conversion, J. Electrochem. Soc. 122 (1975) 101–107. doi:10.1149/1.2134132.

[8] M. Mortier, A. Monteville, G. Patriarche, G. Maze, F. Auzel, New progresses in transparent rare-earth doped glass-ceramics, Opt. Mater. (Amst). 16 (2001) 255–267. doi:10.1016/S0925-3467(00)00086-0.

[9] F. Enrichi, C. Armellini, S. Belmokhtar, A. Bouajaj, A. Chiappini, M. Ferrari, A. Quandt, G.C. Righini, A. Vomiero, L. Zur, Visible to NIR downconversion process in Tb3+-Yb3+codoped silica-hafnia glass and glass-ceramic sol-gel waveguides for solar cells, J. Lumin. 193 (2018) 44–50. doi:10.1016/j.jlumin.2017.08.027.

[10] A. Bouajaj, S. Belmokhtar, M.R. Britel, C. Armellini, B. Boulard, F. Belluomo, A. Di Stefano, S. Polizzi, A. Lukowiak, M. Ferrari, F. Enrichi, Tb3+/Yb3+ codoped silica-hafnia glass and glass-ceramic waveguides to improve the efficiency of photovoltaic solar cells, Opt. Mater. (Amst). 52 (2016) 62–68. doi:10.1016/j.optmat.2015.12.013.

[11] L. Zur, C. Armellini, S. Belmokhtar, A. Bouajaj, E. Cattaruzza, A. Chiappini, F. Coccetti, M. Ferrari, F. Gonella, G.C. Righini, E. Trave, A. Vomiero, F. Enrichi, Comparison between glass and glass-ceramic silica-hafnia matrices on the down-conversion efficiency of Tb3+/Yb3+ rare earth ions, Opt. Mater. (Amst). 87 (2019) 102–106. doi:10.1016/j.optmat.2018.05.008.

[12] G. Boulon, Why so deep research on Yb3+-doped optical inorganic materials?, J. Alloys Compd. 451 (2008) 1–11. doi:10.1016/j.jallcom.2007.04.148.

[13] Y.-J. Liang, F. Liu, Y.-F. Chen, X.-J. Wang, K.-N. Sun, Z. Pan, New function of the Yb3+ ion as an efficient emitter of persistent luminescence in the short-wave infrared, Light Sci. Appl. 5 (2016) e16124. doi:10.1038/lsa.2016.124.

[14] G. Lakshminarayana, J. Qiu, Near-infrared quantum cutting in RE3+/Yb3+ (RE = Pr, Tb, and Tm): GeO2-B2O3-ZnO-LaF3 glasses via downconversion, J. Alloys Compd. 481 (2009) 582–589. doi:10.1016/j.jallcom.2009.03.034.

[15] Y. Katayama, S. Tanabe, Downconversion for 1μm luminescence in lanthanide and Yb3+-codoped phosphors, in: F. Enrichi, G.C. Righini (Eds.), Sol. Cells Light Manag. Mater. Strateg. Sustain., Elsevier, 2019.

[16] G. Alombert-Goget, C. Armellini, S. Berneschi, A. Chiappini, A. Chiasera, M. Ferrari, S. Guddala, E. Moser, S. Pelli, D.N. Rao, G.C. Righini, Tb3+/Yb3+ co-activated Silica-Hafnia glass ceramic waveguides, Opt. Mater. (Amst). 33 (2010) 227–230. doi:10.1016/j.optmat.2010.09.030.

[17] X. Liu, S. Ye, Y. Qiao, G. Dong, B. Zhu, D. Chen, G. Lakshminarayana, J. Qiu, Cooperative downconversion and near-infrared luminescence of Tb3+-Yb3+codoped lanthanum borogermanate glasses, Appl. Phys. B Lasers Opt. 96 (2009) 51–55. doi:10.1007/s00340-009-3478-z.

[18] X. Zhou, Y. Wang, G. Wang, L. Li, K. Zhou, Q. Li, Cooperative downconversion and near-infrared luminescence of Tb 3+/Yb3+ co-doped tellurite glass, J. Alloys Compd. 579 (2013) 27–30. doi:10.1016/j.jallcom.2013.05.058.

[19] J.-L. Yuan, X.-Y. Zeng, J.-T. Zhao, Z.-J. Zhang, H.-H. Chen, X.-X. Yang, Energy transfer mechanisms in Tb3+ , Yb3+ codoped Y2O3 downconversion phosphor, J. Phys. D Appl. Phys. 41 (2008) 105406-1-105406–6. doi:10.1088/0022-3727/41/10/105406.

[20] S. Ye, Z. Guo, H. Wang, S. Li, T. Liu, D. Wang, Evolution of Ag species and molecular-like Ag cluster sensitized Eu3+emission in oxyfluoride glass for tunable light emitting, J. Alloys Compd. 685 (2016) 891–895. doi:10.1016/j.jallcom.2016.06.226.

[21] J.A. Jiménez, S. Lysenko, H. Liu, E. Fachini, C.R. Cabrera, Investigation of the influence of silver and tin on the

luminescence of trivalent europium ions in glass, J. Lumin. 130 (2010) 163–167. doi:10.1016/j.jlumin.2009.08.007.

[22] A.E. Abbass, H.C. Swart, R.E. Kroon, Effect of silver ions on the energy transfer from host defects to Tb ions in sol-gel silica glass, J. Lumin. 160 (2015) 22–26. doi:10.1016/j.jlumin.2014.11.037.

[23] J. Li, R. Wei, X. Liu, H. Guo, Enhanced luminescence via energy transfer from Ag+ to RE ions (Dy3+, Sm3+, Tb3+) in glasses, Opt. Express. 20 (2012) 10122–10127. doi:10.1364/oe.20.010122.

[24] F. Enrichi, S. Belmokhtar, A. Benedetti, A. Bouajaj, E. Cattaruzza, F. Coccetti, E. Colusso, M. Ferrari, P. Ghamgosar, F. Gonella, M. Karlsson, A. Martucci, R. Ottini, P. Riello, G.C. Righini, E. Trave, A. Vomiero, S. You, L. Zur, Ag nanoaggregates as efficient broadband sensitizers for Tb3+ ions in silica-zirconia ion-exchanged sol-gel glasses and glass-ceramics, Opt. Mater. (Amst). 84 (2018) 668–674. doi:10.1016/j.optmat.2018.07.074.

[25] H. Lin, D. Chen, Y. Yu, R. Zhang, Y. Wang, Molecular-like Ag clusters sensitized near-infrared down-conversion luminescence in oxyfluoride glasses for broadband spectral modification, Appl. Phys. Lett. 103 (2013) 091902. doi:10.1063/1.4819951.

[26] E. Trave, M. Back, E. Cattaruzza, F. Gonella, F. Enrichi, T. Cesca, B. Kalinic, C. Scian, V. Bello, C. Maurizio, G. Mattei, Control of silver clustering for broadband Er3+luminescence sensitization in Er and Ag co-implanted silica, J. Lumin. 197 (2018) 104–111. doi:10.1016/j.jlumin.2018.01.025.

[27] A. Martucci, M. De Nuntis, A. Ribaudo, M. Guglielmi, S. Padovani, F. Enrichi, G. Mattei, P. Mazzoldi, C. Sada, E. Trave, G. Battaglin, F. Gonella, E. Borsella, M. Falconieri, M. Patrini, J. Fick, Silver-sensitized erbium-doped ion-exchanged sol-gel waveguides, Appl. Phys. A Mater. Sci. Process. 80 (2005) 557–563. doi:10.1007/s00339-004-2967-5.

[28] C. Strohhöfer, A. Polman, Silver as a sensitizer for erbium, Appl. Phys. Lett. 81 (2002) 1414–1416. doi:10.1063/1.1499509.

[29] P. Mazzoldi, S. Padovani, F. Enrichi, G. Mattei, C. Sada, E. Trave, M. Guglielmi, A. Martucci, G. Battaglin, E. Cattaruzza, F. Gonella, C. Maurizio, Sensitizing effects in Ag-Er co-doped glasses for optical amplification, in: Proc. SPIE 5451. Integr. Opt. Photonic Integr. Circuits, 2004: pp. 311–326. doi:10.1117/12.549912.

[30] F. Enrichi, E. Cattaruzza, M. Ferrari, F. Gonella, R. Ottini, P. Riello, G.C. Righini, E. Trave, A. Vomiero, L. Zur, Ag-Sensitized Yb3+ Emission in Glass-Ceramics, Micromachines. 9 (2018) 1–7. doi:10.3390/mi9080380.

[31] F. Enrichi, E. Cattaruzza, T. Finotto, P. Riello, G.C. Righini, E. Trave, A. Vomiero, Ag-Sensitized NIR-Emitting Yb3+-Doped Glass-Ceramics, Appl. Sci. 10 (2020) 2184. doi:10.3390/app10062184.

[32] F. Enrichi, C. Armellini, G. Battaglin, F. Belluomo, S. Belmokhtar, A. Bouajaj, E. Cattaruzza, M. Ferrari, F. Gonella, A. Lukowiak, M. Mardegan, S. Polizzi, E. Pontoglio, G.C. Righini, C. Sada, E. Trave, L. Zur, Silver doping of silica-hafnia waveguides containing Tb3+/Yb3+ rare earths for downconversion in PV solar cells, Opt. Mater. (Amst). 60 (2016) 264–269. doi:10.1016/j.optmat.2016.07.048.

[33] F. Enrichi, E. Cattaruzza, M. Ferrari, F. Gonella, A. Martucci, R. Ottini, P. Riello, G.C. Righini, E. Trave, A. Vomiero, L. Zur, Investigation of the role of Ag multimers as broadband sensitizers in Tb3+/Yb3+ co-doped glass-ceramics, in: Proc. SPIE 10683. Fiber Lasers Glas. Photonics Mater. through Appl., 2018: p. 106830T. doi:10.1117/12.2314738.

[34] F. Enrichi, E. Cattaruzza, P. Riello, G.C. Righini, A. Vomiero, Ag-sensitized Tb3+/Yb3+ codoped silica-zirconia glasses and glass-ceramics: Systematic and detailed investigation of the broadband energy-transfer and downconversion processes, Ceram. Int. 47 (2021) 17939–17949. doi:10.1016/J.CERAMINT.2021.03.107.

[35] X. Zhao, D. Vanderbilt, Phonons and lattice dielectric properties of zirconia, Phys. Rev. B - Condens. Matter Mater. Phys. 65 (2002) 075105. doi:10.1103/PhysRevB.65.075105.

[36] H. Jiang, R.I. Gomez-Abal, P. Rinke, M. Scheffler, Electronic band structure of zirconia and hafnia polymorphs from the GW perspective, Phys. Rev. B. 81 (2010) 851119. doi:10.1103/PhysRevB.81.085119.

[37] L.R. Doolittle, Algorithms for the rapid simulation of Rutherford backscattering spectra, Nucl. Instruments Methods Phys. Res. Sect. B Beam Interact. with Mater. Atoms. 9 (1985) 344–351. doi:10.1016/0168-583X(85)90762-1.

[38] S. Enzo, S. Polizzi, A. Benedetti, Applications of fitting techniques to the Warren-Averbach method for X-ray line broadening analysis, Zeitschrift Fur Krist. - New Cryst. Struct. 170 (1985) 275–287. doi:10.1524/zkri.1985.170.1-4.275.

[39] P. Li, I.-W. Chen, J.E. Penner-Hahn, Effect of Dopants on Zirconia Stabilization-An X-ray Absorption Study: I, Trivalent Dopants, J. Am. Ceram. Soc. 77 (1994) 118–128. doi:10.1111/j.1151-2916.1994.tb06964.x.

[40] P. Li, I. -W Chen, J.E. Penner-Hahn, Effect of Dopants on Zirconia Stabilization—An X-ray Absorption Study: II, Tetravalent Dopants, J. Am. Ceram. Soc. 77 (1994) 1281–1288. doi:10.1111/j.1151-2916.1994.tb05403.x.

[41] P. Li, I. -W Chen, J.E. Penner-Hahn, Effect of Dopants on Zirconia Stabilization—An X-ray Absorption Study:

III, Charge-Compensating Dopants, J. Am. Ceram. Soc. 77 (1994) 1289–1295. doi:10.1111/j.1151-2916.1994.tb05404.x.

[42] A. Sobolev, A. Musin, G. Whyman, K. Borodianskiy, O. Krichevski, A. Kalashnikov, M. Zinigrad, Stabilization of cubic phase in scandium-doped zirconia nanocrystals synthesized with sol-gel method, J. Am. Ceram. Soc. 102 (2019) 3236–3243. doi:10.1111/jace.16232.

[43] F.L. Cumbrera, G. Sponchia, A. Benedetti, P. Riello, J.M. Pérez-Mato, A.L. Ortiz, Some crystallographic considerations on the novel orthorhombic ZrO2 stabilized with Ta doping, Ceram. Int. 44 (2018) 10362–10366. doi:10.1016/j.ceramint.2018.03.048.

[44] Y.S. Vidya, K. Gurushantha, H. Nagabhushana, S.C. Sharma, K.S. Anantharaju, C. Shivakumara, D. Suresh, H.P. Nagaswarupa, S.C. Prashantha, M.R. Anilkumar, Phase transformation of ZrO2:Tb3+ nanophosphor: Color tunable photoluminescence and photocatalytic activities, J. Alloys Compd. 622 (2015) 86–96. doi:10.1016/J.JALLCOM.2014.10.024.

[45] P.N. Sen, M.F. Thorpe, Phonons in AX2 glasses: From molecular to band-like modes, Phys. Rev. B. 15 (1977). doi:10.1103/PhysRevB.15.4030.

[46] F.L. Galeener, Band limits and the vibrational spectra of tetrahedral glasses, Phys. Rev. B. 19 (1979). doi:10.1103/PhysRevB.19.4292.

[47] M. Okuno, N. Zotov, M. Schmücker, H. Schneider, Structure of SiO2-Al2O3 glasses: Combined X-ray diffraction, IR and Raman studies, in: J. Non. Cryst. Solids, 2005. doi:10.1016/j.jnoncrysol.2005.01.014.

[48] A. Feinberg, C.H. Perry, Structural disorder and phase transitions in ZrO2-Y2O3 system, J. Phys. Chem. Solids. 42 (1981). doi:10.1016/0022-3697(81)90032-9.

[49] S.W. Lee, R.A. Condrate, The infrared and Raman spectra of ZrO2-SiO2 glasses prepared by a sol-gel process, J. Mater. Sci. 23 (1988). doi:10.1007/BF00547474.

[50] M. Wang, J. Cheng, M. Li, F. He, Raman spectra of sodalimesilicate glass doped with rare earth, Phys. B Condens. Matter. 406 (2011). doi:10.1016/j.physb.2011.07.014.

[51] M.T. Wang, J.S. Cheng, M. Li, F. He, Structure and properties of soda lime silicate glass doped with rare earth, Phys. B Condens. Matter. 406 (2011). doi:10.1016/j.physb.2010.10.040.

[52] T. Merle, R. Guinebretiere, A. Mirgorodsky, P. Quintard, Polarized Raman spectra of tetragonal pure ZrO2 measured on epitaxial films, Phys. Rev. B - Condens. Matter Mater. Phys. 65 (2002). doi:10.1103/PhysRevB.65.144302.

[53] J. Cai, C. Raptis, Y.S. Raptis, E. Anastassakis, Temperature dependence of Raman scattering in stabilized cubic zirconia, Phys. Rev. B. 51 (1995). doi:10.1103/PhysRevB.51.201.

[54] H. Lamb, On the vibrations of an elastic sphere, Proc. London Math. Soc. 13 (1881) 189–212. doi:10.1112/plms/s1-13.1.189.

[55] A. Tamura, K. Higeta, T. Ichinokawa, Lattice vibrations and specific heat of a small particle, J. Phys. C Solid State Phys. 15 (1982) 4975. doi:10.1088/0022-3719/15/24/010.

[56] M. Isogai, A. Veber, D. de Ligny, M.R. Cicconi, T. Hayakawa, Devitrification behavior of sol-gel derived ZrO2-SiO2 rare-earth doped glasses: Correlation between structural and optical properties, Ceramics. 1 (2018). doi:10.3390/ceramics1020022.